A Geostationary Optical Seismometer, Proof of Concept

R. Michel, J.-P. Ampuero, J.-P. Avouac, N. Lapusta, S. Leprince, D.C. Redding and S. N. Somala

Abstract—**We discuss the possibility of imaging the propagation of seismic waves from a very large space-based optical telescope. Images of seismic waves propagating at the Earth's surface would be an invaluable source of information for investigating earthquake physics and the effect of the subsurface on earthquake ground motions. This application would require ground displacement measurements at about every 100 m, with centimetric accuracy, and temporal sampling on the order of 1 Hz. A large field of view (>10^5 km^2) is required to measure the full extent of a large earthquake in the areas of interest. A geostationary optical telescope with a large aperture appears to be the most promising system. We establish preliminary technical requirements for such a system, which lead us to consider a telescope with an angular field of view of 0.8 degree and with an aperture greater than 4 m. We discuss and quantify the various sources of noise that would limit such a system: atmospheric turbulence; evolution of ground reflectance and solar incidence angle; and stability of the platform at 1 Hz. We present numerical simulations, which account for these sources of noise. They show that key details of the seismic wave field, hardly detectable using ground-based instruments, would indeed be imaged by such a system. Data flow would be about 20-50 Gb.s^{-1} and data memory about 50 Tb, at the upper limit of modern technology.**

Index Terms—**Geophysical deformations, large space telescope, geostationary, earthquakes, subpixel, correlation, optical flow, photoclinometry, Earth monitoring**

I. Introduction

A number of geophysical processes can produce displacements at the Earth's surface over a wide range of time and length scales. These processes include tectonics (earthquakes, transient slow slip, volcanic eruptions); geomorphology (landslides, soil creep, sand dunes migration); and glaciology (calving and flow of mountain

Manuscript received ***. Part of this research was supported by the French Centre National des Etudes Spatiales and funded through the TOSCA program. Part of this research was carried out at the Jet Propulsion Laboratory, California Institute of Technology, under a contract with the National Aeronautics and Space Administration, and funded through the internal Research and Technology Development.

R. Michel is now at Institut des Sciences de la Terre de Paris, Université Pierre et Marie Curie. J.-P. Ampuero, J.-P. Avouac, N. Lapusta, S. Leprince and S.N. Somala are with the California Institute of Technology, Department of Geology and Planetary Science, Pasadena, CA 91160 USA (phone: 626-***-****; fax: 626 ***-****; e-mail: remi.michel@upmc.fr). D.C. Redding is with the Jet Propulsion Laboratory, California Institute of Technology, MS 306-438, California Institute of Technology, 4800 Oak Grove Drive, Pasadena, CA 91109

glaciers and ice caps). Remote sensing has proven effective for observing these processes ([1-3]). However, some of them are very transient, and investigating their dynamics would require a temporal resolution greatly exceeding the capabilities of any existing space-based system. Indeed, current systems are limited to a monthly, or at best to a daily sampling. Ground based instruments (e.g., continuously recording GPS receivers, seismometers or accelerometers) can provide a good temporal resolution, but systematic monitoring of large areas (e.g., the entire state of California, or the Pacific coast of the Americas) with high spatial resolution (100 m to 1 km) would require an unaffordable effort of instrument deployment and maintenance. Here we explore the possibility of such monitoring based on remote sensing. On the application side, we focus on the possibility of measuring seismic waves, as such measurements would bring unprecedented insight into earthquake physics, which remain poorly understood, and on the effect of sub-surface structures on seismic waves, a major factor controlling damage intensity during large earthquakes [4, 5]. This application is most challenging due to the transient and faint nature of seismic waves: large earthquakes typically last between a few tens of seconds and a few minutes; seismic waves travel at velocities on the order of a few kilometers per second and generate surface displacements of typically a few centimeters to a few tens of centimeters, e.g., [6]. The development of physics-based earthquake models is necessary to improve our ability to develop realistic earthquake scenarios and assess their probability of occurrence. At the moment, in absence of such a foundation, seismic hazard studies are based on simple conceptual models of the seismic cycle on faults which have little physical grounds and observations which are too incomplete to assess the full range of possible earthquakes scenarios in the future. Well constrained source models (the time evolution of seismic slip on the fault) are necessary to develop and test earthquake source models. The determination of earthquake sources from currently available seismological and geodetic measurements of ground motion is a vastly ill-posed problem. A denser coverage in space and time of ground displacement should allow overcoming that limitation and help constrain spatial variations of elastic properties at depth which are know to be a major factor controlling the distribution of earthquake damages.

Low altitude imaging sensors, onboard drones or stratospheric balloons, would provide fields of view that are too narrow. They would also present stability issues for this particular application, which requires extremely accurate registration at all times. Low and Medium Earth Orbiters only offer a limited temporal monitoring due to their apparent motion; constellations of satellites have been proposed to overcome this issue [7, 8] but tens of platforms would be required for the proposed application. A geostationary orbit seems a better option, as it would allow near-continuous, large field of view imagery. A geostationary radar would either require an extremely large monolithic antenna of kilometric scale, or would allow producing only a couple of Synthetic Aperture Radar images a day [9].

In the following, we therefore focus on the potential of a very large optical geostationary telescope. We consider more specifically the case of the San Andreas Fault System in California (Fig. 1). There, the seismicity is indeed quite active and characterized by frequent and shallow strike-slip earthquakes. The probability of observing measurable events in in this area of high interest is relatively large. We also introduce a pointing strategy for the spacecraft that would allow it to image earthquakes occurring anywhere along the Pacific coast of the Americas, between 50°S and 50°N, raising the number of large earthquakes (M>6) that can be measured to 2.3 per year.

Hereafter, we first introduce the main characteristics of California seismicity and the associated seismic waves. We use these to derive preliminary requirements for the design of a space-based imager. We review useful fundamental concepts in atmospheric optics and photometry, and discuss the various sources of noise that could affect the capability of the telescope to detect seismic waves. We analyze the potential of two possible techniques to measure both the horizontal and the vertical ground motion induced by seismic waves. The horizontal and vertical motions are retrieved from the sequences of images using optical-flow and photoclinometry techniques, respectively. Preliminary elements of a mission design, including optics, detection, data handling and pointing strategy are then presented.

II. Preliminary Seismological Requirements

A. Characteristics of Southern California Seismicity

Southern California has experienced a total of 46 earthquakes with magnitude M_w greater than 5 over the decade 1990-2000. The largest event over that period, the Landers earthquake in 1992, reached a magnitude 7.3 (Fig. 1) [10]. It is estimated that Southern California has more than 99% chance of experiencing a M_w >6.5 earthquake over the next 30 years, and an 80% chance of a M_w >7.0 earthquake [11]. Those events are mostly strike-slip earthquakes, producing predominantly horizontal shear displacements at the Earth’s surface. Earthquakes with magnitudes larger than 6.5 generally produce surface ruptures, while smaller earthquakes do not. These characteristics make California an appealing target for the proposed monitoring system.

B. Characteristics of seismic waves

Seismic waves generated by earthquakes depend on the source characteristics as well as on propagation effects [6]. They typically propagate at speeds of kilometers per second and the particle velocity at the ground surface is typically on the order of centimeters per second or above in the epicentral area. Ground motion recordings provided by seismological stations are routinely exploited to derive earthquake source models (e.g., [12]) or to image subsurface variations of elastic properties (e.g., [13]). Capturing details of the wave field pattern that might reveal the physics of seismic ruptures has remained a challenge, however.

Imaging seismic waves with dense sampling both in time and space would provide seismologists with a fundamentally new type of data. As an illustration, Fig. 2 shows the ground motion generated by a typical dynamic rupture simulation of a strike slip earthquake of magnitudes M_w 7 [14]. This particular source model involves a super-shear rupture front, i.e. rupture fronts that propagate faster than shear waves: a sonic boom-like wave front [12, 15, 16] is indeed identifiable as a Mach cone. This phenomenon has been observed in analogue experiments [15] and has been inferred to occur during some large earthquakes, although never through the sort of direct observations that could be afforded with a dense observational system. These simulations illustrate patterns of seismic wave propagation that are not recoverable from sparse ground instrumentation and which, if measured, would provide invaluable insight into earthquake source physics.

Fig. 2 also shows versions of the earthquake scenario scaled down to M_w 6 and 5. Here we assume that the fault rupture reached the surface in all cases and that the observations have a broad frequency band. Under these conditions, an important characteristic of seismic waves, resulting from the self-similarity of earthquake sources, is that the peak ground velocity does not depend much on the magnitude of the earthquake. A change in magnitude essentially results in a change of spatial scale as illustrated in Fig. 2.

C. *Preliminary Seismological Requirements on the Instrument*

Our goal is to measure surface deformation between successive images acquired at an appropriate sampling rate and ground spatial resolution, so that the wave field generated by earthquakes of magnitude M_w 5 or above would be measurable. We focus on a sampling rate of 1 Hz, the nominal (and optimistic) high frequency limit of conventional earthquake source imaging studies, which arises from the inaccuracy of synthetic Green's functions due to large uncertainties on the fine-scale structure of the crust. We estimate that independent measurements of ground displacement at about every 100 m, with a measurement accuracy of about 1 cm, would be required. The proposed accuracy allows measurement of ground velocities up to distances of a few rupture lengths away from the fault, a near-source range with high information content to infer fault slip. The proposed spatial sampling is several times finer than the shortest wavelengths (at 1 Hz) that propagate in the shallowest layers of the crust with low seismic wave velocities of several 100 m.s^{-1}. Such requirements place tight constraints on the exposure time. Indeed, as waves propagate over the surface at an apparent speed of up to three kilometers per second, the integration time needs to be lower than about 0.03 s for consistency with a spatial sampling of about 100 m.

Finally, the instrument field of view needs to be large enough to cover the main area of activity being studied. For a satellite that is pointed solely at Southern California, the needed field is about 500×250 km^2. As discussed below, however, a different pointing strategy, one that reacts to earthquakes detected by ground seismometers to identify foreshocks, is able to point the spacecraft with a higher likelihood of success. The field of view required if this approach is followed can be somewhat smaller.

III. MEASURABLE QUANTITIES FROM OPTICAL IMAGES

A. *Horizontal and Vertical Components of Surface Deformation*

Surface deformation induced by seismic waves locally affects both the photometry and the geometry of the images acquired from a geostationary telescope. The horizontal displacement of the ground induces geometrical distortion of the images that may be recovered by various tracking techniques, for example by image cross-correlation. In that case, the measured quantity would be the two horizontal components of the local ground displacement increment between successive images.

Seismic waves also produce vertical displacements, which can induce a photometric effect measurable by photoclinometry, or "shape-from-shading", procedures. The tilt associated with the horizontal gradient of vertical ground displacements locally modifies the solar incidence angle and thus the photometric budget. Changes in the reflected light are measured and spatially integrated to estimate the component in the solar incident plane of the incremental displacement between successive images (Fig. 3).

B. *Useful Photometry and Geometrical Optics Considerations*

In this section, we estimate the number *I* of photons detected by the optical telescope and we derive the photometric equation for the images. Spectral radiances ($W.sr^{-1}.m^{-2}.nm^{-1}$) are simulated in the visible-to-shortwave-infrared with a spectral sampling of 10 nm using a direct multiple scattering transfer model [17] with the following entries: aerosol-free, US 1976 Standard Atmosphere Model with a vertical integrated water vapor content equal to 3.25 cm, and varying solar zenith angle.

The radiance L_{toa} at the top of the atmosphere is [18]:

$$L_{toa} = L_{atm} + \frac{E_{ground}}{\pi}.\frac{\rho}{1 - S\rho}.T_{atm} \tag{1}$$

where L_{atm} is the down-top radiance of the atmosphere, E_{ground} is the spectral solar irradiance of the ground ($W.m^{-2}.nm^{-1}$), ρ is the reflectance of the ground, S is the spherical albedo of the atmosphere and T_{atm} the transmittance of the atmosphere.

The average number *I* of detected photons per detector (per image pixel) is then:

$$I = \frac{\pi.c.h}{4\left(f/_D\right)^2}.S_d.\Delta t.\int_{\lambda} T_{opt}.L_{toa}.\rho_d.\frac{1}{\lambda}.d\lambda \tag{2}$$

where T_{opt} is the transmittance of the optics, f is the focal length, D is the diameter of the primary mirror, S_d is the surface of the elementary detector, Δt is the integration time, c the speed of light in vacuum, h the Planck constant, ρ_d the quantum efficiency of the detector and λ is the wavelength. Note that T_{opt}, L_{toa} and ρ_d depend on λ.

It is convenient to use the simple scattering approximation of L_{toa}, that slightly differs from the more accurate multiple scattering (1), in order to estimate the noise and the amplitude of differential photoclinometry:

$$L_{toa} = L_{Sun}.{T_{atm}}^2.\rho.cos(\theta) + L_{atm} \tag{3}$$

where L_{sun} is the solar radiance and θ the solar incidence on the ground. ρ was estimated within the spectral range of the CDD at a sampling rate of 10 nm from MODIS data (visible channels) over the area of interest [19]. The average visible reflectance for the area is 0.18 and the standard deviation is 0.03.

IV. Evaluation of the Various Sources of Noise

We analyze various sources of noise that could obscure the signal induced by seismic waves: meteorology; natural sources of radiance variation; instrumental optical noise, mainly induced by instability of the line of sight of the optics (the so-called jitter); and detection noise.

A. Meteorology, Probability of Clear-Sky Sunny Conditions

A passive optical instrument requires daylight and clear sky weather. Southern California experiences more than 291 days of clear sky per year, that is 80% [20].

B. Sun and Sun Incidence

The shot noise induced by the statistical fluctuation of detected photons is a Poisson process and the associated noise σ_{Sun} on I is the square root of I.

The solar irradiance of the ground, and thus the image, depend on the sun incidence angle (3). Because of the relatively low latitude of California, the sun incidence angle varies there from 90 to a minimum of about 10 degrees from zenith. We have considered that the telescope will work with a maximum sun incidence angle θ_{max} equal to 80 degrees from zenith. This limits the observation condition to an average of 10 hours per day.

Moreover, during the acquisition of images, the Earth rotates so that the solar incidence angle changes. This effect induces an extremely low relative variation of I ((2) and (3)) of about 2×10^{-6} per second. For applications, which would not require a sampling rate as high as 1 Hz, this effect would be more significant. For example, the relative variation of I between images acquired one minute apart is on the order of 5×10^{-3}, which is of the same order as for images acquired exactly 24 hours apart.

Because of the constraints on the irradiance of the ground described above, the theoretical probability that the telescope will image a particular earthquake is about 33% (that is 291 days per year and 10 hours per day).

C. Atmospheric Turbulence

We consider both the phase and amplitude effects of atmospheric turbulence on the image: because of the atmospheric turbulence, the light received by the telescope is impacted by both wavefront error and scintillation [21].

The atmospheric turbulence layer is a well known source of geometric distortions in the case of ground based telescopes [21]-[28]. The effect is small for a telescope in a geostationary orbit, 36,000 km away from the Earth surface. The magnitude of this effect can be calculated by integrating the turbulence profile over the optical path, accounting for the propagation geometry, and is normally expressed in terms of Fried's atmospheric coherence length r_0 [25] for a spherical wave

$$r_0{}^{-5/3} = 0.423\left(\frac{2\pi}{\lambda}\right)^2 \int_0^L C_n^2(z).\left(\frac{z}{L}\right)^{5/3} dz \tag{4}$$

where λ is wavelength, C_n^2 is the turbulence structure parameter, and the integral is from a point on the ground to the altitude L of the telescope. Using a Hufnagel-Valley 5/7 model for the C_n^2 profile [26], r_0 is ~360 m at geostationary altitude – much larger than the telescope diameter – indicating that turbulence will have only very small effects on the image.

To compute the apparent ground motion of a patch of diameter *D* caused by turbulence, we can use the fact that the turbulent layer is very thin compared to the propagation distance to the satellite in order to simplify the problem, and assume the apparent patch diameter is approximately constant throughout the atmosphere. The variance σ_t^2 of the one dimensional tilt of a beam of diameter *D* propagating through an atmosphere of height h_{atm} is given by [24]

$$\sigma_t = 3.0\, D^{-1/3} \int_0^{h_{atm}} C_n^2(z)dz \tag{5}$$

If the turbulence were in a thin layer at height h_0, then the rms translation of the beam σ_x – the apparent patch motion for this application – would be just $\sigma_x = \sigma_t h_0$. For 1 arcsec seeing, the tilt for meter-class apertures is $\sigma_t \sim$ 1.5 urad, and for effective atmospheric height $h_0 \sim 10$ km, the projected ground motion is ~1.5 cm rms for this simple model. More accurately, for an arbitrary turbulence profile, we can sum the translation over the turbulent layers, yielding [22]

$$\sigma_x^2 = 3.0D^{-1/3} \int_0^{h_{atm}} C_n^2(h)h^2dh \tag{6}$$

Using the Hufnagel-Valley 5/7 model for C_n (r_0 = 5 cm, 7 urad isoplanatic angle) [26], and assuming 21 m/sec for high altitude wind speed, the integral is evaluated, and the result expressed as rms apparent motion in m:

$$\sigma_x \cong 0.008\, D^{-1/6} \tag{7}$$

so that for a 1 m patch on the ground, the translation is ~0.8 cm rms. Over a correlation patch ~100 m wide, the apparent motion is less than ~0.4 cm rms; hence this source of noise is negligible.

Less negligible with regard to photoclinometry is the irradiance fluctuation σ_{scint} induced by atmospheric turbulence, known as scintillation [27]. We use the Rytov approximation, a wavelength of 1 micrometer, the Hufnagel-Valley turbulence model and a point source because of the incoherent light. Weak fluctuations are expected because $r_0 > \sqrt{\lambda L}$ [19]. The normalized irradiance variance σ_{Scin} at the primary mirror of the telescope can be estimated as [28]:

$$\left(\frac{\sigma_{scin}}{I}\right)^2 = 2.25\left(\frac{2\pi}{\lambda}\right)^{7/6} \int_0^{L} C_n^2(z)\left(1-\frac{z}{L}\right)^{\frac{5}{6}} z^{5/6}dz \tag{8}$$

The normalized irradiance variance is estimated from (8) to be about 0.02 which is definitely characteristic of a weak turbulence. Because the normalized irradiance variance estimated for the telescope's entrance pupil is 0.02, it has very little effect on image quality. The total energy of this noise corresponds to about 2% of the shot noise σ_{Sun} considered above.

D. *Bidirectional Reflectance Distribution Function of the Ground*

The bidirectional reflectance distribution function (BRDF) is defined as the ratio of reflected radiance to incoming irradiance as a function of the incoming solar incidence angle and of the outgoing viewing angle with respect to the reflector surface's normal. The BRDF is a four-dimensional function that defines how light is reflected at an opaque surface. A local change of the BRDF changes ρ and thus the photometric budget of the images according to (1). Because of the rotation of the Earth, the solar incidence angle changes from one image to another. Though the BRDF is constant for a Lambertian ground, it may vary in the desert, vegetated and urban contexts that comprise the studied area. The maximum variation estimated for the BRDF of natural scenes is about 1% per degree [29-31]. The variation of the apparent reflectance would thus be at most on the order of 10^{-5} per minute in the context of this study. The effect of BRDF variations is therefore negligible.

Windblown sand and dust, potentially brought in suspension due to ground shaking in the epicentral area, would also change the apparent BRDF. Potential collapse of buildings would also dramatically change the BRDF in urban areas. Those effects are highly context-dependent and are not addressed in this study.

V. Measuring Horizontal Displacements from Correlation or optical Flow

It has already been demonstrated that horizontal displacements can be measured with subpixel accuracy from optical remote sensing images [3, 32-39]. In these studies, horizontal displacements were measured using image cross-correlation, because correlation techniques can be made insensitive to the strong variations of contrasts that often characterize images of natural scenes acquired days, months, or years apart. In the case of a geostationary satellite acquiring images at the high temporal frequency envisioned here, the variation of contrast with time may be very low, thus allowing easier estimation of the displacement of the images with time. Thus, optical flow techniques are of interest [35], as they yield subpixel accuracy when there is very good photometric stability between images. In the previous section, we have shown that images acquired less than 1s apart would present a relative radiometric stability better than 2×10^{-6}. This would theoretically contribute to a noise level on the measurement of horizontal displacements lower than $1/1000^{th}$ of the pixel size from optical flow [36]. The reported accuracy in current gradient-based optical flow estimation is, however, not better than $1/10^{th}$ to $1/100^{th}$ of a pixel [35]. Better accuracy would require further development, including calibration of the detectors at the subpixel scale.

Several factors limit the performance of correlation and optical flow techniques. These need to be evaluated in the context of this study. On the sensor side, they include aliasing, quantization, non-uniform CCD response to viewing angle, electronic noise and inaccuracies of the correlation and optical flow procedures [40]. On the object side, they include differences in viewing and sun incidence angles, uncertainty on the topography, sparse self-affine distribution of optical scatters in natural scenes [41] and temporal decorrelation of the scene.

State of the art procedures have achieved accuracy better than $1/10^{th}$ of the pixel size on real data [3, 36-39, 42, 43], mainly from the opportunistic use of images acquired with different solar incidences and viewing angles, with variation as large as 40 degrees; 1 byte in quantization and temporal decorrelation over decades.

A geostationary telescope acquiring high quality images dedicated to the estimate of ground displacements should perform significantly better. We can conclude, from the previous sections, that the residual noise on the estimate of the deformation from geostationary imagery, induced by uncertainty on the topography, difference on solar incidence angle and temporal change from atmospheric turbulence, would be about a few 1/1000th of the pixel size. This is equivalent to a negligible noise on ground displacements, typically of a few millimeters for a telescope of diameter larger than about 4 m and corresponding to a ground resolution finer than 6 m.

For the reasons outlined above, we find that correlation processing of images acquired in the present context should yield a noise on the estimate of the displacement on the order of 1/100th of the pixel size (rms), when averaged over the correlation window size of 100 m square, with data quantization of about 10 bits.

VI. Measuring Near Vertical Displacements from photoclinometry

Photoclinometry is a shape-from-shading technique commonly used to derive surface topography from images, interpreting variations in brightness as being induced by changes in solar incidence angle due to variations of surface slope (ground tilt). It is mainly used in glaciology and planetary science [44-48]. Analysis of the variation of intensity in the image provides the component of the surface slope in the solar incidence plane. The topography is then recovered using spatial integration.

In this section we analyze the potential of photoclinometry to estimate the near vertical component of seismic waves. We thus only consider the transient surface topography induced by the earthquake. In the following, we use first order estimates of the photometric budget to derive the noise level expected for photoclinometry of propagating seismic waves; detailed equations of photoclinometry can be found in [43]. Because this technique does not rely on correlation, we suppose that the ground resolution of the images, *GR*, used for photoclinometry, is the same as the spatial resolution requested for the displacement map (about 100 m). The transient topography modifies the local slope of the ground and thus the solar incidence on the ground θ. Differentiation of (3) with respect to θ yields:

$$\Delta L \approx \rho L_{Sun} T_{atm}^{2} sin(\theta) \Delta\theta \tag{9}$$

Estimate of topography from photoclinometry might be very complex in variable land covers mainly because measured radiances depend on two unknown parameters that are the ground reflectance and the incidence angle. In this application, that is differential photoclinometry, we take benefit of the very small variations of the incidence induced by earthquakes in order to mitigate this difficulty. Because L_{atm} is typically an order of magnitude below $\rho L_{Sun} T_{atm}^{2}$ in the visible, we assume from (9), in order to estimate the level of noise, that

$$\Delta\theta \approx \frac{\Delta L}{\rho L_{Sun} T_{atm}^{2} sin(\theta)} \approx \frac{\Delta L}{L.\tan\theta} \approx \frac{\Delta I}{I.\tan\theta} \tag{10}$$

Estimation of $\Delta z = GR.\Delta\theta$ from (10) with accuracy in the 1 to 10 cm range would require very good stability of the relative irradiance, $\Delta I/_I$, in the 10^{-5} to 10^{-4} range at mid-solar azimuth of about 34 degrees. Thus, while the correlation procedure requires very good spatial resolution, photoclinometry requires very good photometric accuracy.

The noise $\sigma(\Delta z)$ on Δz can be estimated from (10):

$$\sigma(\Delta z) \approx \frac{GR}{I.tan(\theta)}.(\sigma_{Sun} + \sigma_{stab} + \sigma_{detec}) \tag{11}$$

Where σ_{stab} is the noise on I induced by the changes in the line of sight and σ_{detec} is the detection noise. The instrument could benefit from a highly stabilized line of sight now achievable with recent systems such as the James Webb Space Telescope [49]. For pointing stability θ_{stab} in the range of 1 milliarcsec at 1 Hz, corresponding to a relative displacement on the ground ($L.\theta_{stab}$) of about 17 cm, σ_{stab} would be:

$$\sigma_{stab} \approx L.\theta_{stab}.|gradI| \tag{12}$$

$|gradI|/I$ is considered to be independent of the spatial scale due to the self-affine property of natural scenes [36] and has been estimated on Landsat images of the area of interest to be equal to 2%. σ_{detec} is on the order of 10 electrons for advanced CCD detectors and is not significant for this application.

From (11) and (12) we find that $\sigma(\Delta z)$ is 9 cm for the case of a 4 m telescope and an incidence angle of 10 degrees. To achieve this accuracy, quantization of the measured flux should be about 16 bits, in order to measure the small variations of I. In practice, this requirement will limit accurate photoclinometry to areas that receive direct illumination from the Sun.

VII. ELEMENTS OF MISSION DESIGN

A. *Pointing Strategy*

Two different strategies could be adopted regarding the pointing of the instrument. The telescope could be dedicated to the monitoring of a single zone known to have a high probability of yielding useful signal, such as southern California. This approach has the advantage of assuring that earthquakes in this area of prime interest would be seen, but the disadvantage that there are few such earthquakes.

An alternative strategy, one that would allow observation of many more earthquakes, is being explored [50]. This strategy reacts to earthquakes detected by ground seismometers, slewing the satellite to point at the epicenters of earthquakes above a certain magnitude, say 5. Some of these earthquakes will be foreshocks of large earthquakes. With the spacecraft pointed in the right direction, these would be observed. For example, placing the spacecraft in a geostationary orbit over the Pacific coast of the Americas, observations could be made from southern Chile to Southern Alaska. Analysis of the history of earthquakes in this region suggests that by following this strategy, the spacecraft would observe an average of 3 earthquakes of magnitude 6 or larger each year [47]. This strategy would also be effective even with a smaller field of view, 0.4 degrees or even less.

B. Telescope

Given our preliminary requirements on spatial resolution, radiometric sensitivity and horizontal displacement measurement accuracy (whether from correlation or optical flow), we estimate that the primary mirror should at minimum be 4 m wide. While there is no example of such a large telescope for Earth Observation, at least one is currently in development for astronomical observations, the 7 m wide JWST [51]. In the following we show simulations computed assuming a 4 m and a 10 m telescope.

To carry out the first observational strategy, we consider a field of view that completely covers Southern California from a geostationary orbit. Such a field of view would be very large (500×250 km^2, or about 0.8 degree). Providing good image quality over that full field of view presents an interesting optical design challenge. It will also require very large detectors in the focal plane. To avoid aliasing, the focal plane pixel sampling should permit near-critical sampling of the diffraction-limited Point Spread Function. The cutoff frequency of the telescope's optical transfer function is $\lambda f/(2D)$ and the Nyquist criterion requires two samples per period of the highest frequency.. The 500×250 km^2 field of view would hence be composed of 10 Gpixels for the 4 m telescope and up to 56 Gpixels for the 10 m telescope. The corresponding ground sample distance (pixel sampling) for the 4 and 10 m telescopes would be about 3.6 m and 1.5 m, respectively.

The field of view could be substantially smaller if the second observational strategy is followed: 300 km by 150 km, say. This is still a very large field, requiring billions of pixels: 3.5 Gpixels for the 4 m telescope. Temporal sampling should be in the range of 1-2 Hz. Billion pixel cameras have already been developed [52, 53] and the instrument could benefit from state-of-the-art high back-side illuminated CCD or CMOS detectors, with high quantum efficiency, high pixel QE uniformity, low read noise (~10 electrons), vertical anti-blooming [54-56], high full well capacity, high linearity and very low image persistence [57, 58].

C. Data Handling

The data flow rate required to support correlation processing would be in the range 20 Gb.s^{-1} to 50 Gb.s^{-1}, assuming 2 Hz temporal sampling (so as to image surface deformation at 1 Hz). On-board data storage of about 20 Tb to 50 Tb would be utilized to store data sequences up to 100 s long, compatible with the typical duration of M_w 7 earthquakes. These would be downlinked at a slower rate. Photoclinometry would utilize the same data, downsampled after downlink to 100 m to match the lower spatial resolution required. Downsampling will also increase the quantization to 16 bits or better over the larger 100 m sampling area.

The very large data flow rate required to readout full frames at 80 Gb.s^{-1} is an engineering challenge. Currently, the giga-pixel camera of the LSST allows a frame rate of 0.5 Hz [59] and the performances of space-based data storage units already exceeds 6 Tb in memory capacity, with input data rate better than 0.5 Gb.s^{-1} [60]. The management of the full data is thus achievable, but it should be noticed that data flow could be significantly reduced by data compression, such as by transferring irradiance variations only: areas of equal irradiance with respect to a *SNR* of say 1000 for correlation or optical flow could be determined and not sampled. An archive of data could also be recorded over the year and a predictive Kalman filter could help to reduce the data flow.

D. Stability

The stability of line of sight of the telescope can be considered at temporal frequencies either above or below the readout rate. Instability of line of sight at frequencies greater than 1-2 Hz will induce a blur reducing the effective spatial resolution. Instability at lower frequencies would induce a uniform shifting of the images. The state of the art in pointing stability of the line-of-sight of space based telescopes is of a few milliarcsec at 1 Hz, in the case of the James Webb Space Telescope [49]. Such stability corresponds to 0.17 cm on the ground or 3 and 10% of the pixel size for primary mirrors of 4 m and 10 m, respectively. The associated blur and global shift would be of that order and thus would not contribute significantly to noise on estimated components of the displacement vector. The blur would yield a reduction in ground resolution lower than few percents. Any global shift could easily be measured and compensated. The impact on photometry has been shown to be lower than 1 cm.

VIII. Conclusions and Perspectives

Fig. 3 and 4 show the simulation of the seismic wave field that might be measured with a 10 m or a 4 m telescope. These simulations were computed using the same scenarios as those depicted in Fig. 2 and accounting for the various sources of noise discussed in the text. We have used additive white Gaussian noise models with variance associated to the various sources of noise discussed above. The horizontal components of the seismic wave field are assumed to be measured from image correlation or optical flow with the performance described above. The vertical component of the seismic wave field is assumed to be measured from photoclinometry, also based on the parameters discussed above. It is seen that both techniques should be able to provide images of the wavefield with sufficient resolution that the key features of the source might be retrieved. Though estimates obtained from the 4 m telescope are somewhat noisy, most of the useful signal is recovered, including the Mach cone and high spatial frequency patterns resulting from the transition from a subshear to a supershear rupture. Based on this simulation, the photoclinometric technique looks particularly promising while the accuracy (9cm) is does not reach preliminary requirements expressed by seismologists (Fig. 4). In fact, because photoclinometry yields spatially dense measurements, the accuracy of each measurement does not need to be as good as the 1cm required for sparsely distributed GPS stations.

While the area of prime seismological interest in this study is California, a much larger area – the Pacific coast of the Americas – is actually accessible from the satellite. Following our second, reactive strategy for pointing the satellite – using ground seismometry to identify possible foreshocks, and staring at these regions – will provide data for 2.3 large earthquakes per year on average, from Southern Alaska to Southern Chile [47]. This data would provide unique insight into earthquake source physics and seismic wave propagation effects, encompassing California and other seismically active areas.

The position of the spacecraft, its high optical quality, large field of view and large field of regard will make it an ideal platform for other scientific studies. The same data could be simply reused for other studies. If different data, such as multi-spectral data, is required, additional instruments could share the telescope.

Preliminary requirements on the accuracy of the measurement (1 cm) have been derived on the basis of sparsely distributed measurements by ground-based seismic and GPS networks. The very high spatial density of the measurements provided by the telescope may help releasing part of this constraint. More precise estimate of the requirements, crucial for the definitive estimate of the diameter of the optical aperture, is being pursued, continuing the work begun in this study.

This study thus shows that the concept of a Geostationnary Optical Telescope to image seismic waves holds promise, although all possible limiting factors have not been considered here and some aspects of the study certainly await more thorough analysis. For simplicity, the models presented here assume a planar fault in a homogeneous elastic half-space. In reality, faults are never exactly planar and the propagation medium is heterogeneous, so that actual wavefields would show distortions and complexities related to both the rupture dynamics and the propagation effects. New seismological methods are being developed that would take advantage of the measurements proposed here to allow discrimination of source and propagation effects.

The study of other types of geophysical deformations would also benefit from a very large space based telescope. Most of these studies would be far less demanding in terms of data rate and field of view. It could be envisioned in order to monitor volcanic eruptions, landslides, soil creep, sand dunes migration, calving and flow of mountain glaciers and ice caps, depending on cloud cover. A very large telescope may also be of major interest to monitor coastal areas, including water quality shallow bathymetry. However, because the locations of interest may be outside Southern California it may be necessary to develop either a repointing capability or a very large field of view. A pointing capability is necessary to carry out the second observational strategy in any event. The design of a very large field, large aperture telescope (up to 4×4 degrees, covering more than 2000×2000 km^2 on the ground), could be envisioned on the basis of the design of the Large Space Survey Telescope [61, 62].

ACKNOWLEDGMENT

Authors thank Mark M. Colavita from the Jet Propulsion Laboratory for his detailed and very helpful comments about turbulence.

REFERENCES

[1] D. Massonnet and K. L. Feigl, "Radar interferometry and its application to changes in the earth's surface", *Reviews of Geophysics*, vol. 36, pp. 441-500, Nov 1998.

[2] A. Kaab, "Monitoring high-mountain terrain deformation from repeated air- and spaceborne optical data: examples using digital aerial imagery and ASTER data", *ISPRS Journal of Photogrammetry and Remote Sensing,* vol. 57, pp. 39-52, Nov 2002.

[3] N. Van Puymbroeck, R. Michel, R. Binet, J. P. Avouac, and J. Taboury, "Measuring earthquakes from optical satellite images", *Applied Optics,* vol. 39, pp. 3486-3494, Jul 10 2000.

[4] T. E. Lay, Aster, R., Forsyth, D., Romanowicz, B., et al., "Seismological Grand Challenges in Understanding Earth's Dynamic Systems", Report to the National Science Foundation, IRIS Consortium, 2009.

[5] National Research Council (U.S.). Committee on Earth Science and Applications from Space: A Community Assessment and Strategy for the Future., *Earth science and applications from space : national imperatives for the next decade and beyond*. Washington, DC: National Academies Press, 2007.

[6] T. Lay and T. C. Wallace, *Modern global seismology*. San Diego: Academic Press, 1995.

[7] D. Massonnet, "Capabilities and limitations of the interferometric cartwheel", *Geoscience and Remote Sensing, IEEE Transactions on,* vol. 39, pp. 506-520, 2001.

[8] T. Amiot, F. Douchin, E. Thouvenot, J. C. Souyris, and B. Cugny, "The interferometric cartwheel: a multi-purpose formation of passive radar microsatellites", in *Geoscience and Remote Sensing Symposium, 2002. IGARSS '02. 2002 IEEE International*, 2002, pp. 435-437 vol.1.

[9] D. Bruno, S. E. Hobbs, and G. Ottavianelli, "Geosynchronous synthetic aperture radar: Concept design, properties and possible applications", *Acta Astronautica,* vol. 59, pp. 149-156, Jul-Sep 2006.

[10] S. C. E. D. C. (SCEDC). [Online]. Available at: http://www.data.scec.org/catalog_search/date_mag_loc

[11] W. G. o. C. E. Probabilities, "The Uniform California Earthquake Rupture Forecast, Version 2 (UCERF 2)", 2008.

[12] A. O. Konca, S. Leprince, J. P. Avouac, and D. V. Helmberger, "Rupture Process of the 1999 M-w 7.1 Duzce Earthquake from Joint Analysis of SPOT, GPS, InSAR, Strong-Motion, and Teleseismic Data: A Supershear Rupture with Variable Rupture Velocity", *Bulletin of the Seismological Society of America,* vol. 100, pp. 267-288, Feb 1 2010.

[13] C. Tape, Q. Y. Liu, A. Maggi, and J. Tromp, "Adjoint Tomography of the Southern California Crust", *Science,* vol. 325, pp. 988-992, Aug 21 2009.

[14] Y. Kaneko, N. Lapusta, and J. P. Ampuero, "Spectral element modeling of spontaneous earthquake rupture on rate and state faults: Effect of velocity-strengthening friction at shallow depths", *Journal of Geophysical Research-Solid Earth,* vol. 113, pp. -, Sep 27 2008.

[15] K. Xia, A. J. Rosakis, and H. Kanamori, "Supershear and subrayleigh to supershear transition observed in laboratory earthquake experiments", *Experimental Techniques,* vol. 29, pp. 63-66, May-Jun 2005.

[16] M. Bouchon and M. Vallee, "Observation of long supershear rupture during the magnitude 8.1 Kunlunshan earthquake", *Science,* vol. 301, pp. 824-826, Aug 8 2003.

[17] C. Miesch, L. Poutier, W. Achard, X. Briottet, X. Lenot, and Y. Boucher, "Direct and inverse radiative transfer solutions for visible and near-infrared hyperspectral imagery", *IEEE Transactions on Geoscience and Remote Sensing,* vol. 43, pp. 1552-1562, Jul 2005.

[18] K.-N. Liou, *An introduction to atmospheric radiation*, 2nd ed. Amsterdam ; Boston: Academic Press, 2002.

[19] W. L. Barnes, T. S. Pagano, and V. V. Salomonson, "Prelaunch characteristics of the Moderate Resolution Imaging Spectroradiometer (MODIS) on EOS-AM1”, *Geoscience and Remote Sensing, IEEE Transactions on,* vol. 36, pp. 1088-1100, 1998.

[20] S. L. Horstmeyer, *The Weather Almanac: A Reference Guide to Weather, Climate, and Related Issues in the United States and Its Key Cities*, 2010.

[21] L. C. Andrews, *Field guide to atmospheric optics*. Bellingham, Wash.: SPIE Press, 2004.

[22] J. H. Churnside and R. J. Lataitis, "Wander of an Optical Beam in the Turbulent Atmosphere”, *Applied Optics,* vol. 29, pp. 926-930, Mar 1 1990.

[23] M. Colavita, "Ground scene translation from space attributable to optical turbulence”, JPL, internal memorandum, September 8 2011.

[24] R. J. Noll, "Zernike Polynomials and Atmospheric-Turbulence”, *Journal of the Optical Society of America,* vol. 66, pp. 207-211, 1976.

[25] D. L. Fried, "Statistics of a Geometric Representation of Wavefront Distortion”, *Journal of the Optical Society of America,* vol. 55, pp. 1427-&, 1965.

[26] F. Roddier, "Effects of Atmospheric-Turbulence on the Formation of Visible and Infrared Images”, *Journal of Optics-Nouvelle Revue d'Optique,* vol. 10, pp. 299-303, 1979.

[27] L. C. Andrews, "An Analytical Model for the Refractive-Index Power Spectrum and Its Application to Optical Scintillations in the Atmosphere”, *Journal of Modern Optics,* vol. 39, pp. 1849-1853, Sep 1992.

[28] M. Sechaud, F. Mahe, T. Fusco, V. Michau, and J. M. Conan, "High resolution imaging through atmospheric turbulence: link between anisoplanatism and intensity fluctuations”, *Optics in Atmospheric Propagation and Adaptive Systems III,* vol. 3866, pp. 100-109, 1999.

[29] C. A. Russell, J. R. Irons, and P. W. Dabney, "Bidirectional reflectance of selected BOREAS sites from multiangle airborne data”, *Journal of Geophysical Research-Atmospheres,* vol. 102, pp. 29505-29516, Dec 26 1997.

[30] J. R. Irons, G. S. Campbell, J. M. Norman, D. W. Graham, and W. M. Kovalick, "Prediction and Measurement of Soil Bidirectional Reflectance”, *IEEE Transactions on Geoscience and Remote Sensing,* vol. 30, pp. 249-260, Mar 1992.

[31] G. Meister, A. Rothkirch, H. Spitzer, and J. K. Bienlein, "Large-scale bidirectional reflectance model for urban areas”, *IEEE Transactions on Geoscience and Remote Sensing,* vol. 39, pp. 1927-1942, Sep 2001.

[32] J. P. Avouac, F. Ayoub, S. Leprince, O. Konca, and D. V. Helmberger, "The 2005, M-w 7.6 Kashmir earthquake: Sub-pixel correlation of ASTER images and seismic waveforms analysis”, *Earth and Planetary Science Letters,* vol. 249, pp. 514-528, Sep 2006.

[33] F. Ayoub, S. Leprince, and J. P. Avouac, "Co-registration and correlation of aerial photographs for ground deformation measurements”, *ISPRS Journal of Photogrammetry and Remote Sensing,* vol. 64, pp. 551-560, Nov 2009.

[34] S. Dominguez, J. P. Avouac, and R. Michel, "Horizontal coseismic deformation of the 1999 Chi-Chi earthquake measured from SPOT satellite images: Implications for the seismic cycle along the western foothills of central Taiwan", *Journal of Geophysical Research-Solid Earth,* vol. 108, pp. -, Feb 7 2003.

[35] Y. Klinger, R. Michel, and J. P. Avouac, "Co-seismic deformation during the M-w 7.3 Aqaba earthquake (1995) from ERS-SAR interferometry", *Geophysical Research Letters,* vol. 27, pp. 3651-3654, Nov 2000.

[36] S. Leprince, S. Barbot, F. Ayoub, and J. P. Avouac, "Automatic and precise orthorectification, coregistration, and subpixel correlation of satellite images, application to ground deformation measurements", *IEEE Transactions on Geoscience and Remote Sensing,* vol. 45, pp. 1529-1558, Jun 2007.

[37] S. Leprince, P. Muse, and J. P. Avouac, "In-flight CCD distortion calibration for pushbroom satellites based on subpixel correlation", *IEEE Transactions on Geoscience and Remote Sensing,* vol. 46, pp. 2675-2683, Sep 2008.

[38] R. Michel and J. P. Avouac, "Deformation due to the 17 August 1999 Izmit, Turkey, earthquake measured from SPOT images", *Journal of Geophysical Research-Solid Earth,* vol. 107, pp. -, Apr 10 2002.

[39] R. Michel and J. P. Avouac, "Coseismic surface deformation from air photos: The Kickapoo step over in the 1992 Landers rupture", *Journal of Geophysical Research-Solid Earth,* vol. 111, pp. -, Mar 21 2006.

[40] V. N. Dvornychenko, "Bounds on (Deterministic) Correlation-Functions with Application to Registration", *IEEE Transactions on Pattern Analysis and Machine Intelligence,* vol. 5, pp. 206-213, 1983.

[41] D. L. Turcotte, *Fractals and chaos in geology and geophysics*, 2nd ed. Cambridge, U.K. ; New York: Cambridge University Press, 1997.

[42] H. C. Liu, T. H. Hong, M. Herman, T. Camus, and R. Chellappa, "Accuracy vs efficiency trade-offs in optical flow algorithms", *Computer Vision and Image Understanding,* vol. 72, pp. 271-286, Dec 1998.

[43] J. W. Brandt, "Improved accuracy in gradient-based optical flow estimation", *International Journal of Computer Vision,* vol. 25, pp. 5-22, Oct 1997.

[44] D. G. Jankowski and S. W. Squyres, "Sources of Error in Planetary Photoclinometry", *Journal of Geophysical Research-Planets,* vol. 96, pp. 20907-20922, Nov 25 1991.

[45] A. S. Mcewen, "Photometric Functions for Photoclinometry and Other Applications", *Icarus,* vol. 92, pp. 298-311, Aug 1991.

[46] K. Watson, *Photoclinometry from spacecraft images*. Washington,: U.S. Govt. Print. Off., 1968.

[47] B. Horn and M. J. Brooks, *Shape from shading*. Cambridge, Mass.: MIT Press, 1989.

[48] R. L. Kirk, "A fast finite-element algorithm for two-dimensional photoclinometry", Ph.D., Caltech, 1987.

[49] A. J. Bronowicki, "Vibration isolator for large space telescopes", *Journal of Spacecraft and Rockets,* vol. 43, pp. 45-53, Jan-Feb 2006.

[50] J. J. Redding, "Observational Strategies for a Geostationary Seismic Imager Space Telescope", Independent study project, 2011.

[51] J. Gardner, J. Mather, M. Clampin, R. Doyon, M. Greenhouse, H. Hammel, J. Hutchings, P. Jakobsen, S. Lilly, K. Long, J. Lunine, M. McCaughrean, M. Mountain, J. Nella, G. Rieke, M. Rieke, H.-W. Rix, E. Smith, G. Sonneborn, M. Stiavelli, H. Stockman, R. Windhorst, and G. Wright, "The James Webb Space Telescope", *Space Science Reviews,* vol. 123, pp. 485-606, 2006.

[52] H. Yan and S. Yang, "A MODIS dual spectral rain algorithm", *Journal of Applied Meteorology and Climatology,* vol. 46, pp. 1305-1323, Sep 2007.

[53] V. Radeka, J. Frank, J. C. Geary, D. K. Gilmore, I. Kotov, P. O'Connor, P. Takacs, and J. A. Tyson, "LSST sensor requirements and characterization of the prototype LSST CCDs", *Journal of Instrumentation,* vol. 4, pp. -, Mar 2009.

[54] S. E. Holland, W. F. Kolbe, and C. J. Bebek, "Device Design for a 12.3-Megapixel, Fully Depleted, Back-Illuminated, High-Voltage Compatible Charge-Coupled Device", *IEEE Transactions on Electron Devices,* vol. 56, pp. 2612-2622, Nov 2009.

[55] N. Crouzet, T. Guillot, F. Fressin, and A. Blazit, "Front- vs. back-illuminated CCD cameras for photometric surveys: a noise budget analysis", *Astronomische Nachrichten,* vol. 328, pp. 805-808, Aug 2007.

[56] D. E. Groom, S. E. Holland, M. E. Levi, N. P. Palaio, S. Perlmutter, R. J. Stover, and M. Wei, "Back-illuminated, fully-depleted CCD image sensors for use in optical and near-IR astronomy", *Nuclear Instruments & Methods in Physics Research Section A-Accelerators Spectrometers Detectors and Associated Equipment,* vol. 442, pp. 216-222, Mar 11 2000.

[57] I. Platais, R. F. G. Wyse, and N. Zacharias, "Deep astrometric standards and Galactic structure", *Publications of the Astronomical Society of the Pacific,* vol. 118, pp. 107-123, Jan 2006.

[58] [Anon], "Decision nears on camera type for LSST", *Laser Focus World,* vol. 39, pp. 13-13, Oct 2003.

[59] P. O'Connor, J. Geary, K. Gilmore, J. Oliver, V. Radeka, and P. Takacs, "Technology of the LSST focal plane", *Nuclear Instruments & Methods in Physics Research Section a-Accelerators Spectrometers Detectors and Associated Equipment,* vol. 582, pp. 902-909, Dec 1 2007.

[60] K. F. Chiang and X. X. Xiong, "Pre-launch characterization of aqua MODIS scan mirror response versus scan angle for thermal emissive bands - art. no. 66771J", *Earth Observing Systems XII,* vol. 6677, pp. J6771-J6771, 2007.

[61] P.-Y. Bely, *The design and construction of large optical telescopes*. New York: Springer, 2003.

[62] C. F. Claver. (2007). *LSST REFERENCE DESIGN*. Available: http://lsst.org/files/docs/LSST-RefDesign.pdf

Fig.1

Active faults and seismicity of Southern California. Dots show locations of the 46 Mw>5 earthquakes reported over the period 1990-2000 in the USGS catalogue (http://www.data.scec.org/catalog_search/date_mag_loc). A geostationary optical system monitoring that area would catch on average 12 earthquakes with magnitude greater than 5 per decade. Stars are the major recent events. Telescope's field of view covers the whole area.

Fig.2

Simulations of ground velocities generated by M_w 7, 6 and 5 earthquakes strike slip earthquakes. The fault runs parallel to the upper edge of the model and the snapshot shows the waves computed a couple of seconds after the onset of the rupture. x is the East-West direction, V_x is the East-West component of the velocity. Amplitude of the gradient of horizontal surface velocities measured parallel to the fault strike direction. Note the Mach cone associated with the super-shear propagation of the rupture to the left. The complex wave train reflects the transition from an initial sub-shear crack-like rupture to a super-shear pulse-like rupture.

Fig.3

Simulation of measured wave fields for a 10 m (top) and 4 m (bottom) telescope. The simulations assume correlation of images acquired 1 second apart and take into account the psf of the optical systems and the various sources of noise described in the text. The 4 m telescope should allow resolving the most salient features of the wave field, which reflect the time evolution of the rupture.

Fig.4

Simulation of measured wave fields for a 10 m (left) and 4 m (right) telescope. z denotes the vertical. The simulations assume photoclinometric measurements of images acquired 1 second apart and take into account the psf of the optical systems and the various sources of noise described in text.

FIG.1 Michel et al.

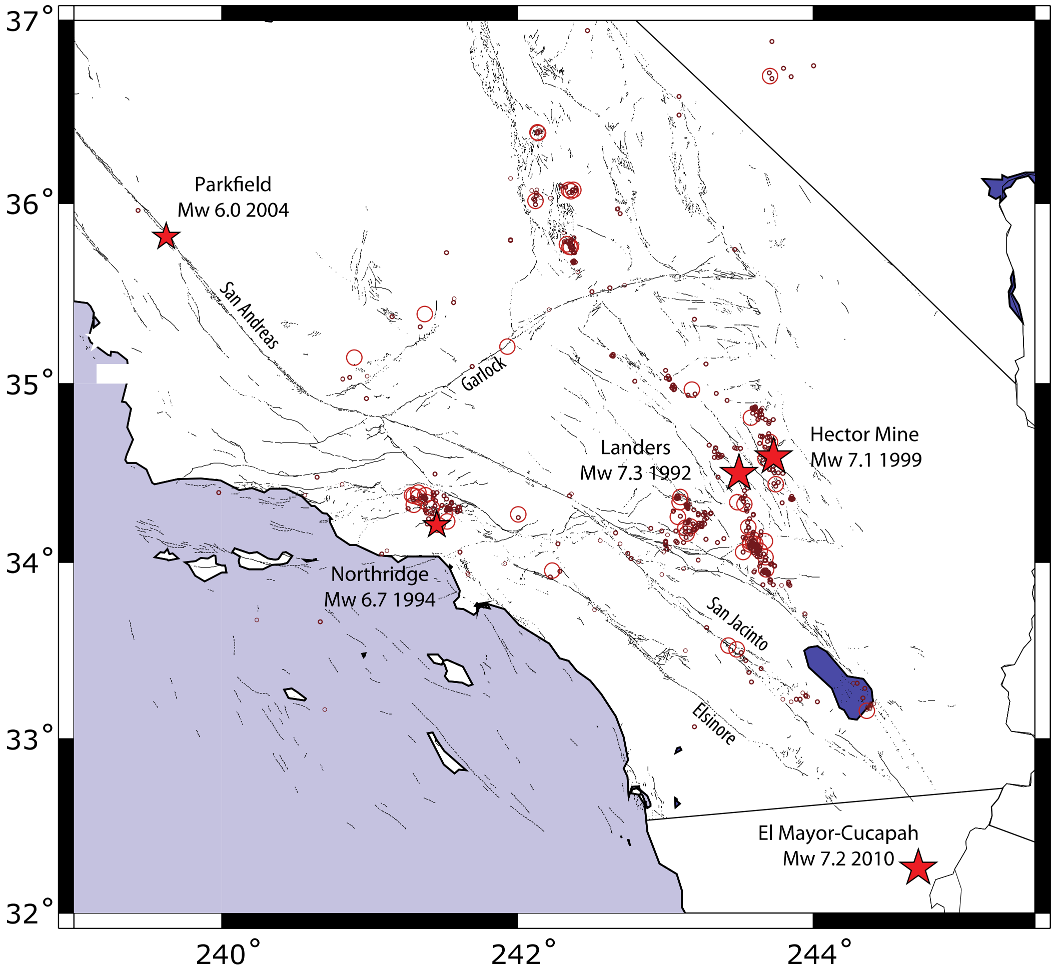

Fig.2

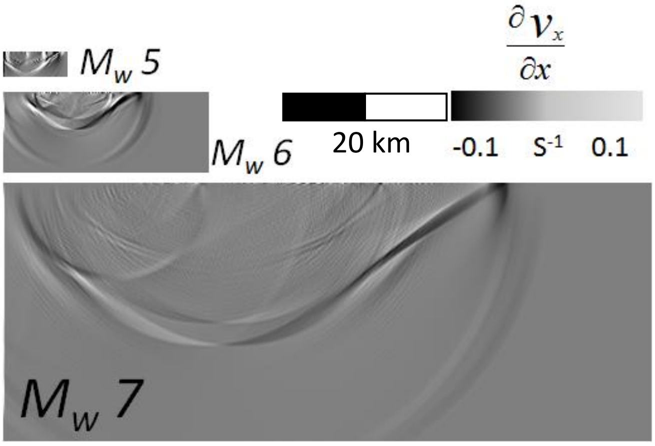

Fig.3

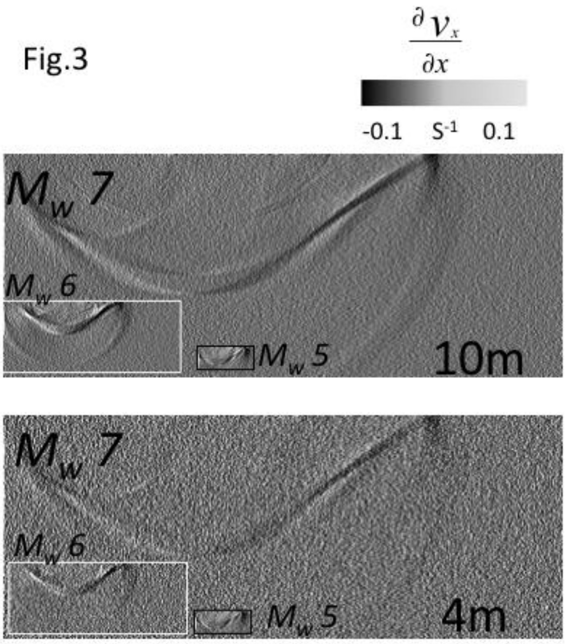
$\frac{\partial v_x}{\partial x}$
-0.1
S^{-1}
0.1
M_w 7
M_w 6
M_w 5
10m
M_w 7
M_w 6
M_w 5
4m

Fig.4